Hydrophobic nanoconfinement enhances CO_2 conversion to H_2CO_3

Nabankur Dasgupta,[1] Tuan A. Ho,[1*] Susan Rempe,[2] and Yifeng Wang[3]

[1]*Geochemistry Department, Sandia National Laboratories, Albuquerque, NM 87185, USA*

[2]*Center for Integrated Nanotechnologies, Sandia National Laboratories, Albuquerque, NM 87185, USA*

[3]*Nuclear Waste Disposal Research and Analysis Department, Sandia National Laboratories, Albuquerque, NM 87185, USA*

* Corresponding author: taho@sandia.gov

Abstract

An understanding of the formation of H_2CO_3 in water from carbon dioxide is important in many environmental, biological, and industrial processes, and in the global carbon cycle. Although numerous computational and experimental investigations have focused on understanding these interactions, the conversion of CO_2 to H_2CO_3 in nanopores, and how this conversion differs from that in bulk water, has not been understood. In this study, we use ReaxFF metadynamics molecular simulations to demonstrate striking differences in the free energy of CO_2 conversion to H_2CO_3 in bulk water compared with that in water confined in pyrophyllite nanopores. We find that the nanoconfinement not only reduces the energy barrier, but also reverses the reaction from endothermic in bulk water to exothermic in nanoconfined water. In addition, charged species are observed more often under nanoconfinement than in bulk water. The higher number of reactive encounters, stronger solvation, and more favorable proton transfer with increasing confinement enhance the thermodynamics and kinetics of the reaction. As carbonation in nanopores is important in the carbon cycle and a complicated problem that depends on confinement, surface chemistry, pore chemistry, and concentration of CO_2, our results provide a mechanistic understanding to an important step in this process.

Introduction

Carbon dioxide (CO_2) is a greenhouse gas that makes a major contribution to global warming and climate change.[1] To reduce CO_2 emissions and mitigate its adverse effects on climate change, several CO_2 management technologies have been developed in recent years, including carbon capture, conversion, and sequestration (CCCS).[2–4] Many of these technologies involve the interaction of clay with CO_2. For example, in geological sequestration, numerous experimental

investigations[5,6] concluded that clay adsorbs a significant amount of CO_2. Natural clay minerals are also potential materials[7,8] for capturing CO_2 due to their large surface area, high porosity, abundant basic sites, excellent thermal and chemical stability, and low cost.[9] Expansive clay minerals, such as montmorillonite, can adsorb a significant amount of water into the interlayers. Therefore, investigation of CO_2 interactions with clay are incomplete without considering the interactions of CO_2 with interlayer water, including the dissolution of CO_2 to form H_2CO_3, which then undergoes dissociation to form bicarbonate (HCO_3^-) and carbonate (CO_3^{2-}) ions, as given by Eq. 1,[10]

$$\mathrm{CO_2 + H_2O \rightleftharpoons H_2CO_3 \rightleftharpoons HCO_3^- + H^+ \rightleftharpoons CO_3^{2-} + 2H^+}. \quad (1)$$

An understanding of the formation of H_2CO_3 in water from carbon dioxide, and its decomposition, is important in many environmental, biological, and industrial processes, and in the global carbon cycle.[11–15] Several studies have examined the formation and dissociation of H_2CO_3 in bulk water by quantum mechanical methods, including density functional theory (DFT), Hartree−Fock (HF), perturbation theories, and enhanced sampling methods. [16] [17] The reaction,

$$CO_2 + nH_2O \rightarrow H_2CO_3 + (n\text{-}1)\ H_2O, \quad (2)$$

specifically the forward reaction for n=1-4 at 0 K, encountered significant energy barriers. For example, when n = 1, the energy barrier is about 50 kcal/mol.[18] Increasing n decreases the energy barrier (at 0 K) to ~33 (n=2), ~29 (n=3), and ~20 kcal/mol (n=4). Independent of n, the energy of H_2CO_3-water complexes is about 6-7 kcal/mol higher than that of the CO_2-water complexes,[18] leading to a more facile reverse Eq. 2 reaction ($H_2CO_3 + nH_2O \rightarrow CO_2$ and $(n+1)H_2O$). Similar to the H_2CO_3 formation reaction from CO_2, adding more water to H_2CO_3 reduces the energy barrier of decomposition significantly,[19–21] from ~44 (n=0) to ~27.1 (n=1) and ~20.9 (n=3) kcal/mol.[21] Other studies[22–24] also found that energy barriers for both forward and reverse hydration reactions decrease to be within the range of 16~20 kcal/mol for n>3, which is in good agreement with experimental values.[25–28]

Even though the thermodynamic and kinetic data for the formation, from CO_2, and dissociation of H_2CO_3 in bulk water are well-known, similar data in nanoconfined water is scarce. It is well-accepted that nanoconfinement can affect properties of water, such as the equation of state,[29,30] phase behavior,[31,32] adsorption,[33,34] dielectric constant,[35–37] and diffusion constant.[38,39] As a result, the reactivity of solutes under nanoconfinement may differ from that in bulk solutions.[40–43] For example, the dimensional reduction and increased fluid density could enhance reactions between small solutes in nanoconfinement,[44,45] whereas reactions involving

large reactants may be sterically hindered.[40] Furthermore, the changes in the parallel and perpendicular component of dielectric tensors of confined water enhance self-dissociation of water even though the quantitative relationship between self-dissociation of water with changes in dielectric tensor remains to be established.[36] Therefore, it is important to elucidate the reactivity of CO_2 under nanoconfinement, which can differ substantially from that in bulk water.

Interlayers of the naturally occurring clay minerals provide a confined environment to augment chemical reaction rates, increase selectivity of species, and stabilize reactive species.[46–48] The clay structural charges and interlayer cations promote a range of physical and chemical processes, including intercalation, swelling, adsorption, and reaction. Experimental[8,49,50] and theoretical (ab initio and classical molecular simulations)[51–56] studies on the interactions among CO_2, water, and clay have focused mainly on adsorption, intercalation, and swelling of clay interlayers. Reactions in Eq. 1 and 2 are poorly investigated in clay nanopores. Limited available data provided a conflicting conclusion about the nanoconfinement effects on CO_2 conversion. For example, Loring et al.[57] and Krukowski et al.[58] found no evidence of carbonate-forming reactions in montmorillonite, while Hur et al.[59] observed the opposite. Only a few studies[60–62] explored the reactivity of CO_2 under different clay interlayers. Those studies reported that the carbonation reaction readily occurs near the electron-rich terminal oxygen sites adjacent to cation vacancies of the surface.Nevertheless, our understanding of the formation of carbonic acid within clay interlayers is incomplete. Further Investigation of carbonic acid formation under nanoconfinement, as pursued here, will help advance our understanding and enable exploitation of CO_2-clay interactions for CCCS.

In this work, we apply an enhanced sampling method, metadynamics, in molecular dynamics simulations using the reactive force field, ReaxFF,[63,64] to investigate the thermodynamics and kinetics of H_2CO_3 formation under nanoconfinement. The ReaxFF molecular simulations allow molecular bonds to be broken and reformed without using expensive quantum mechanical methods. ReaxFF force fields are parameterized according to DFT data and are capable of accurately defining bond formation and bond breaking in large systems (> 10^6 atoms).[65–69] When combined with an enhanced sampling method, ReaxFF molecular simulations can sample high energy states of a relatively large chemically reactive system that would not be possible using ab initio or non-reactive molecular simulations.[70] Therefore, for the present study, ReaxFF metadynamics molecular simulation is deemed to be a reasonable approach for understanding the kinetics and thermodynamics of H_2CO_3 formation in clay interlayers, and comparing with the reaction in the bulk, which has already been studied extensively in the past. Our results reveal striking differences for the reaction in nanopores compared with that in bulk water.

Results and discussions

In Fig. 1, we present the cells used to simulate the reaction of a CO_2 molecule with bulk (Fig. 1a) and confined (Figs. 1b and 1c) water. In Figs. 1b and 1c, there are two (2W) and one (1W) water layers, confined in pyrophyllite (pph) nanopores. Pph is a dioctahedral phyllosilicate ($Al_2Si_4O_{10}(OH)_2$) comprising an octahedral (O) Al-centered sheet sandwiched between two tetrahedral (T) Si-centered sheets (i.e., T-O-T structure). Only one pph layer is explicitly represented in the simulation boxes (Figs. 1b and 1c). When the periodic boundary condition is applied in the *z* direction, water is confined in a pph nanopore. Note that pph does not swell in water; that is, the systems in Figs. 1b and 1c are selected as hypothetical models to investigate the reaction of CO_2 with confined water. This is a reasonable choice as our focus is on the effect of hydrophobic nanoconfinement on the free energy landscape of the conversion of CO_2 to H_2CO_3. In addition, the T-O-T structure of pph can be found in many swelling clays, including montmorillonite.

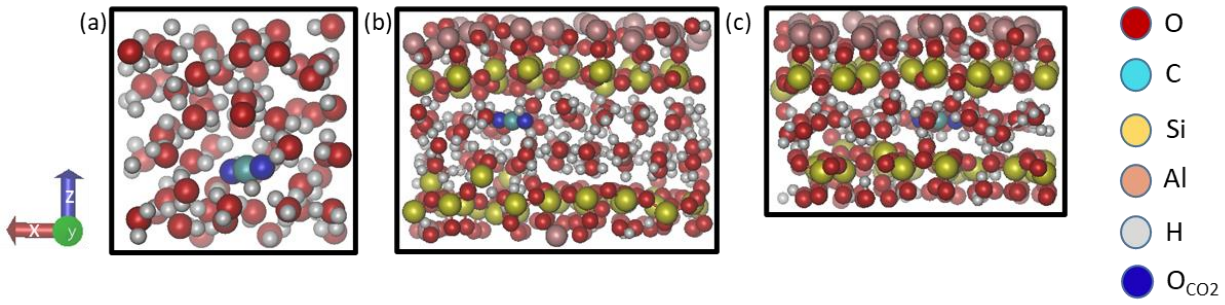

Figure 1: Simulation systems used to investigate the reaction of a CO_2 molecule (cyan-blue colors) with (a) bulk water, and confined water in pyropyllite nanopores consisting of (b) 2W, and (c) 1W layers. The simulation box size for Fig. 1a is 12.5 × 12.5 × 12.5 $Å^3$, with one CO_2 and 64 water molecules. The simulation cell sizes for Figs. 1b and c are 20.64 × 17.93 × 15 $Å^3$ (1 CO_2, 92 H_2O molecules, and a pph surface) and 20.64 × 17.93 × 12 $Å^3$ (1 CO_2 and 54 H_2O molecules, and a pph surface).

The systems in Fig. 1 undergo equilibrium simulations with the ReaxFF force field,[68] as detailed in the computational methods section of the supporting information (SI). After equilibration, the free energy calculations are performed using well-tempered metadynamics,[71] available in the COLVARS[72] package built in the LAMMPS software package.[73] The free energy surfaces (FES, two-dimensional contour plots) represent the free energy for the formation of H_2CO_3 from CO_2 and H_2O as a function of two collective variables, *CV1* and *CV2*, in each environment (bulk and confined water) (see Fig. 2).

The first collective variable, *CV1*, is the coordination number of the carbon in CO_2 (C) and oxygen of water (O_w). The second collective variable, *CV2*, is the coordination number of the oxygen of CO_2 (O_C) and hydrogen of water (H). Variables *CV1* and *CV2* are defined in Eq. 3 and Eq. 4,

$$CV1 = \sum_{k\in \mathrm{O_w}} \frac{1-\left(\frac{r_{\mathrm{CO}_{wk}}}{r_o}\right)^m}{1-\left(\frac{r_{\mathrm{CO}_{wk}}}{r_0}\right)^n} \quad (3)$$

$$CV2 = \sum_{i\in \mathrm{O_C}} \sum_{j\in \mathrm{H}} \frac{1-\left(\frac{r_{ij}}{r_c}\right)^m}{1-\left(\frac{r_{ij}}{r_c}\right)^n} \quad (4)$$

where $r_{\mathrm{CO}_{wk}}$ in Eq. 3 represents the C-O_w (*k* is the number of water molecules) and r_o is the cut-off distance, r_o =1.6 Å. The r_{ij} in Eq. 4 indicates the O_C-H distance [(*i*=1,2) and (*j*=1,2*k*)] and r_c is the cut-off distance for r_{ij}, r_c = 1.3 Å. The exponential factors *m* and *n* have the values of 8 and 16. Small *CV* values (near 0) mean atoms are weakly coordinated while larger values (near 1) indicate strong coordination. More simulation details can be found in the SI.

The FES for the reaction in bulk water (Fig. 2a) comprises two distinguished wells, labeled as R and P, representing the reactant (CO_2 and water complex) and product (H_2CO_3 and water complex). The reaction coordinates (*CV1*, *CV2*) of points R and P are (0.051, 0.103) and (0.936, 0.186). The *CV1* value at point R is small, indicating that the coordination between C and O_w is weak, rendering CO_2 as a mild solvation state (CO_2 is a straight molecule at point R, snapshot R). A high *CV1* value at point P indicates that a C-O_w bond has formed. Once the C-O_w bond forms, proton transfer from any surrounding water molecule to form H_2CO_3 is usually swift and the H_2CO_3 is in a strongly solvated state (snapshot P). Note that formation of carbonic acid is thermodynamically more favorable than bicarbonate and carbonate ions formation.[76,77] We observe the *cis-trans* conformation for H_2CO_3 regardless of the environment, which agrees with the fact that *cis-trans* is the lowest formation free energy out of the three conformers, including *trans-trans* and cis-cis.[23] The point TS at (0.497, 0.178) in Fig. 2a is the transition state. The method used to determine TS is discussed below, and presented in the SI. The TS snapshot in Fig. 2a shows the bending of the O-C-O angle, with a O_w close to the C atom. The O-C-O angle bending is important for H_2CO_3 formation, regardless of solvation environment, and triggered by the C-O_w coordination due to increasing *CV1* value driven by metadynamics simulation. The bending of O-C-O angle in TS of CO_2 and H_2O reaction under bulk environment (see TS in Fig. 2a) agrees well with the overwhelming studies on CO_2 hydration using ab-initio calculations in literature.[18,24,78] There has not been any studies on CO_2 hydration under nanoconfinement as such which can be compared with our present TS configuration inside pph nanopore (see TS in Fig. 2b and Fig. 2c).

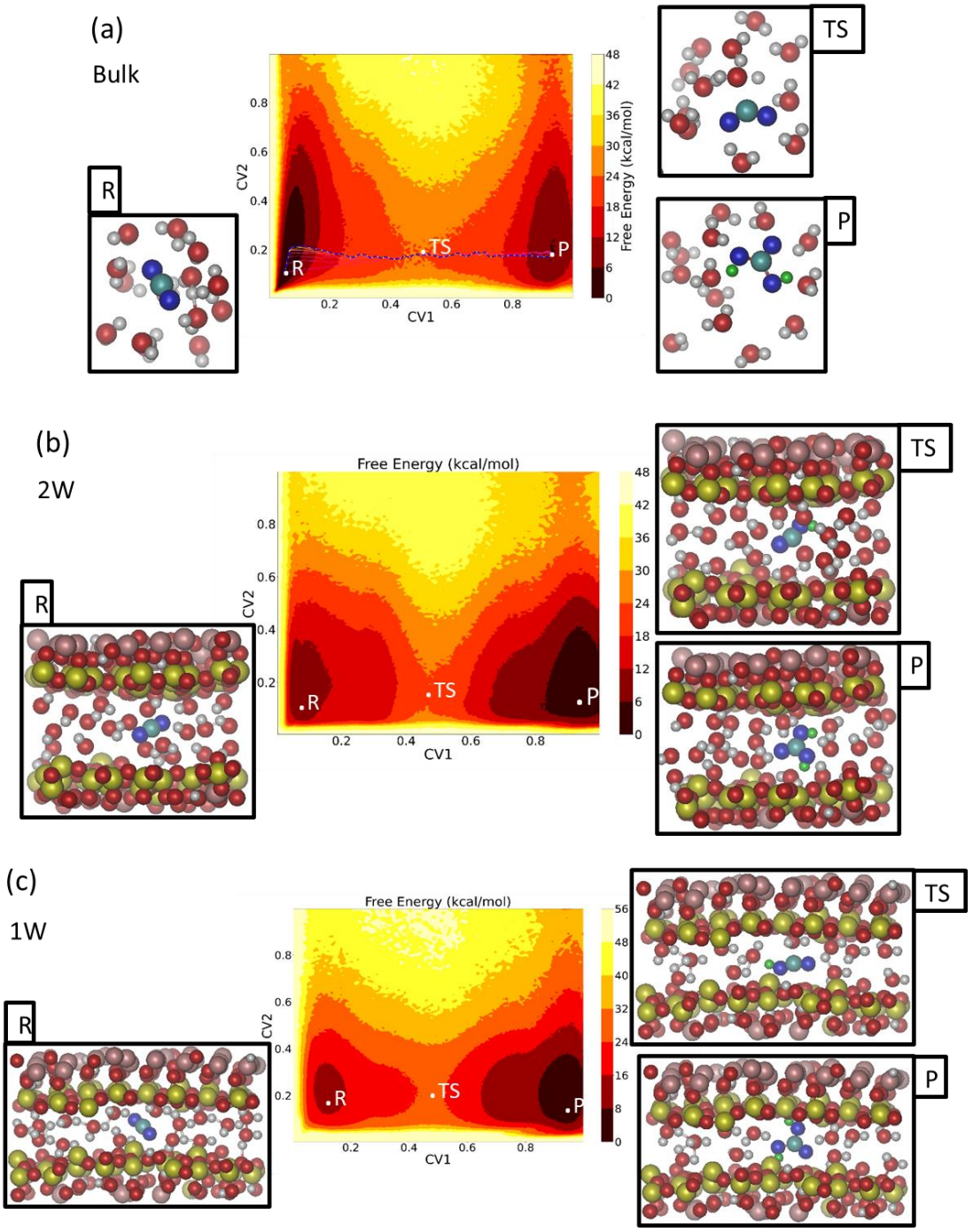

Figure 2: Free energy surface as a function of *CV1* and *CV2* obtained for H_2CO_3 formation in (a) bulk water, and nanoconfined in (b) 2W and (c) 1W layers. The R, P, and TS labels on the FESs and snapshots represent the reactant, product, and transition states in each water environment. The color code is the same as in Fig. 1, except that the H_2CO_3 and TS hydrogens are labelled in green. The blue dashed line on the FES in Fig. 2a is the minimum energy path obtained from the finite temperature string method[74,75] (see SI).

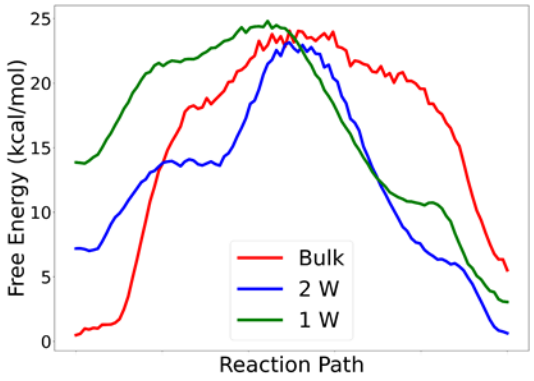

Figure 3: One-dimensional minimum free energy path for reactions in bulk water, and 2W and 1W confined water.

To estimate the free energy barrier and free energy of reaction for H_2CO_3 formation in bulk water, we calculate the one–dimensional minimum energy path (MEP) (dashed blue line on FES in Fig. 2a) using the finite temperature string method (see SI for more details).[74,75] The one-dimensional free energy profile is also reported by the red line in Fig. 3. The energy barrier (difference between energy at TS and that at R) required for H_2CO_3 formation is 23.2 ± 0.43 kcal/mol, which is about 1.4 kcal/mol higher than the experimental value of 21.8 kcal/mol.[27] Our predicted barrier also agrees well with energy barriers calculated previously.[23,27,28] The product is about 4.9 ± 1.36 kcal/mol higher in energy than the reactant (i.e., the well R is deeper than the well P on FES, Fig. 2a; $\Delta G_{\text{bulk}} = 4.9 \pm 1.36\ \text{kcal/mol}$). The geometries and relative free energies between the reactant, transition state, and product computed here are in good agreement with experimental[79] and theoretical studies[18,19,80] for bulk water and carbon dioxide. For example, the gas phase experimental[81,82] and theoretical[18] free energy of formation for H_2CO_3 from CO_2 and H_2O found in prior studies is 4.02 kcal/mol and 5.2 kcal/mol, respectively.

The results obtained for the reaction in pph nanopores are stunningly different from those obtained for the reaction in bulk water. Figs. 2b and 2c show the FES for the same reaction taking place in 2W and 1W pph nanopores. The one-dimensional free energy profiles for 2W and 1W nanopores are reported by the blue and green lines in Fig. 3. These results indicate that, when increasing confinement, the energy barriers decrease from 23.2 ± 0.43 kcal/mol in bulk water to 15.1 ± 3.48 kcal/mol in 2W nanopore, and to 10.4 ± 5.14 kcal/mol in 1W nanopore. Furthermore, the reactant has lower energy than the product ($\Delta G_{\text{bulk}} = 4.9 \pm 1.36\ \text{kcal/mol}$) in bulk water. In contrast, the reactant has higher energy than the product for the reaction in 2W (i.e., the well P is deeper than well R on FES in Fig. 2b, $\Delta G_{2\text{W}} = -6.5 \pm 2.71\ \text{kcal/mol}$) and 1W

pores ($\Delta G_{1\mathrm{W}} = -13.4 \pm 4.33\ \mathrm{kcal/mol}$). This result suggests that hydrophobic nanoconfinement not only reduces the energy barrier, but also changes the thermodynamics of the reaction in favor of product (H_2CO_3) formation. Another difference for the reaction in nanoconfined water, compared with the reaction in bulk water, is that charged species are usually observed in nanopores. Snapshots that represent the TS states in Figs. 2b and 2c already show a proton transferred to the oxygen of CO_2, indicating that the complex formed at TS is a charged species unlike the neutral complex in bulk water (TS state in Fig. 2a).

There are several reasons for the observed differences described above.

First, the free energy barrier is considerably lowered in nanopores compared to bulk water because a water molecule does not bind strongly to the surface under hydrophobic pph nanoconfinement, making it always available near the CO_2 molecule for coordination and reaction. We observe that the free energy required to coordinate water molecules with CO_2 to bend the O-C-O angle of a CO_2 molecule to the O-C-O angle of H_2CO_3 is high, as depicted by the energy barrier (Fig. 2a) to bring the system from R snapshot to TS snapshot. In other words, the reaction requires lower energy to coordinate water molecules with CO_2 in hydrophobic nanopores compared with the energy required to break water hydrogen bonds and coordinate bulk water molecules with a CO_2 molecule. This argument raises questions about the effect of hydrophilicity on the reaction. We will investigate this question in future work with a hypothesis that hydrophilic nanoconfinement will increase the energy barrier compared to energy barriers observed in bulk water and in hydrophobic confined water. Furthermore, steric hindrance imposed by the confining walls favor reactive encounters of the reactants.[40,43] Roughly speaking, confinement leaves only two translational degrees of freedom for the position of one reactant relative to the other, as opposed to three degrees of freedom available in the bulk.

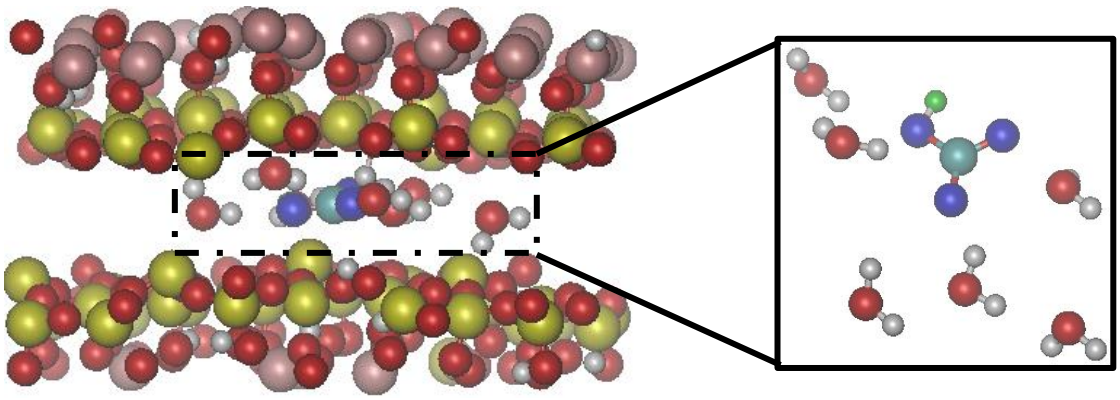

Figure 4: Simulation snapshot demonstrating the formation of a bicarbonate ion in 1W nanopores. The color code is the same as Fig. 2.

Second, the formation of H_2CO_3 from CO_2 and water involves hydrogen transfer that is likely enhanced under nanoconfinement. There is strong evidence that nanoconfinement enhances water self-dissociation,[36] and a qualitative relation between strongly varying components of the dielectric tensor with enhanced self-dissociation.[36] It has also been observed that the parallel component of the dielectric tensor of water at interfaces at ambient conditions increases significantly (up to 120) when approaching the surface from the bulk.[37] The perpendicular component of the dielectric tensor varies only from 0 to 2 upon approaching the interface.[40] We therefore postulate that proton donation to carbon dioxide is more likely in 1W nanopore than in 2W nanopore and in bulk water. In addition, nanoconfinement generically facilitates and stabilizes the formation of charged species.[9][40,43,83] We observe charged species at the TS states (Fig. 2) in nanopores and also the formation of HCO_3^- and H_3O^+ in the nanoconfined regime intermittently before forming H_2CO_3 (Fig. 4). The solvation energy ΔG_s of charged species can be calculated using Born solvation equation

$$\Delta G_s = \omega(1/\varepsilon - 1) \qquad (5)$$

where ω is the Born solvation coefficient, and ε is the dielectric constant. The increase of the parallel component of the dielectric tensor inevitably decreases solvation energy (more negative), while the decrease of the perpendicular component of the dielectric tensor increases solvation energy (less negative). In the 2-dimensional channels (1W and 2W) solvation likely occur in the parallel direction. Therefore, charge species is more likely formed in the nanopores than in bulk water. However, note that bicarbonate ions formed intermittently in solutions due to their high free energy of formation ($\Delta G_{\mathrm{rxn}} = 4.7\ \mathrm{kcal/mol}$) from carbonic acid.[76]

Third, CO_2, the TS, and H_2CO_3 are coordinated by water molecules differently under different environments. We observe that the CV1 value for the state R in nanopores are higher than that in bulk water, indicating a close coordination of C and O_w under hydrophobic nanoconfinement. In other words, a CO_2-confined water complex (at point R, Fig. 2b and 2c) is thermodynamically favorable when the CO_2 molecule is closely coordinated by H_2O molecules, while a CO_2-bulk water complex (at point R, Fig. 2a) is thermodynamically favorable with a looser H_2O - CO_2 coordination. We can imagine the reaction process as follow: (i) water molecules closely coordinate with CO_2 molecule, leading to the O-C-O angle bending (see TS in Fig. 2a), and then (ii) the C-O_w bond forms, followed by proton transfers and hydration of H_2CO_3. The close coordination of CO_2-confined water helps lower the free energy of the first step (i). To further demonstrate the close coordination of CO_2-confined water, in Figure 5a we report the radial distribution function (RDF) of C and O_w at point R for different water environments (see SI for more details on this calculation). The RDF results indicate that, for the 1W case, the first peak (closest C-O_w coordination) is at 2.12 Å. For the 2W case, the first peak is at 2.97 Å. In contrast,

the first peak is at 3.77 Å for bulk water. Similarly, the RDF results for TS and P states (Figs. 5b and 5c) also indicate a close coordination of these states, decreasing in the order 1W > 2W > bulk system.

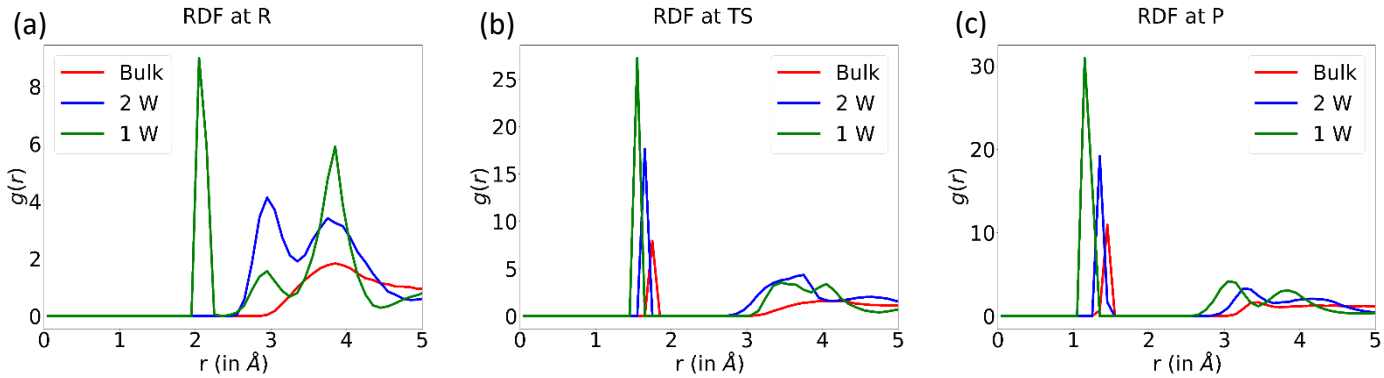

Figure 5: Radial distribution function $g(r)$ for C and O_w atoms in different environments for different states R (a), TS (b), and P (c).

The current research focuses on the CO_2 to H_2CO_3 conversion reaction in hydrophobic nanopores. To complete our understanding of the reactions in Eq. 1 in nanopores, future studies will focus on the same conversion reaction in hydrophilic and heterogeneous nanopores. Certainly, the surface charge distribution and interlayer cations will play a significant role in the thermodynamics and kinetics of the reaction because they can change the solvation and hydrogen bonding properties of the reaction constituents. Finally, the conversion of H_2CO_3 to HCO_3^- and CO_3^{2-} ions in nanopores also needs to be investigated even though those reactions can be much more challenging using the computational method employed here.

Conclusion

We investigated the thermodynamics and kinetics of the conversion of carbon dioxide to carbonic acid in bulk water and in water confined in hydrophobic pph nanopores using ReaxFF metadynamics molecular simulations. Our results demonstrated striking differences for the H_2CO_3 formation in confined water and that in bulk water. The nanoconfined environment not only reduces the energy barrier but also changes the reaction from endothermic in bulk water to exothermic in nanoconfined water. In addition, during the formation of carbonic acid, charged species are observed more often in the nanopores than in bulk water. The increasing number of reactive encounters, improved molecular solvation and coordination, and favored proton transfer with increasing confinement enhances the thermodynamics and kinetics of the reaction.

As carbonation in nanopores is important in the carbon cycle and a complicated problem that depends on confinement, surface and pore chemistry, and concentration of CO_2, our results provide mechanistic understanding to an important step in this process.

Acknowledgement

This article has been authored by an employee of National Technology & Engineering Solutions of Sandia, LLC under Contract No. DE-NA0003525 with the U.S. Department of Energy (DOE). The employee owns all right, title and interest in and to the article and is solely responsible for its contents. The United States Government retains and the publisher, by accepting the article for publication, acknowledges that the United States Government retains a non-exclusive, paid-up, irrevocable, world-wide license to publish or reproduce the published form of this article or allow others to do so, for United States Government purposes. The DOE will provide public access to these results of federally sponsored research in accordance with the DOE Public Access Plan https://www.energy.gov/downloads/doe-public-access-plan. This work was supported by an LDRD project to Tuan A. Ho. This work was performed, in part, at the Center for Integrated Nanotechnologies, an Office of Science User Facility operated for the U.S. Department of Energy (DOE) Office of Science.

The authors declare no competing financial interest.

Keywords: CO_2 conversion, ReaxFF, metadynamics, H_2CO_3 formation, clay interlayer, pyrophyllite, carbon dioxide, bicarbonate ions, carbonate ions, molecular dynamics simulations

References

[1] K. O. Yoro, M. O. Daramola, in (Eds.: M.R. Rahimpour, M. Farsi, M.A.B.T.-A. in C.C. Makarem), Woodhead Publishing, **2020**, pp. 3–28.
[2] Y. Tan, W. Nookuea, H. Li, E. Thorin, J. Yan, *Energy Convers. Manag.* **2016**, *118*, 204–222.
[3] A. Raza, R. Gholami, R. Rezaee, V. Rasouli, M. Rabiei, *Petroleum* **2019**, *5*, 335–340.
[4] Y. Xiong, J. Ye, C. Zhao, *ChemNanoMat* **2021**, *7*, 967–968.
[5] A. Busch, P. Bertier, Y. Gensterblum, G. Rother, C. J. Spiers, M. Zhang, H. M. Wentinck, *Geomech. Geophys. Geo-Energy Geo-Resources* **2016**, *2*, 111–130.
[6] G. M. Bowers, H. T. Schaef, J. S. Loring, D. W. Hoyt, S. D. Burton, E. D. Walter, R. J. Kirkpatrick, *J. Phys. Chem. C* **2017**, *121*, 577–592.
[7] J. Krūmiņš, M. Kļaviņš, R. Ozola-Davidāne, L. Ansone-Bērtiņa, *Miner.* **2022**, *12*, DOI 10.3390/min12030349.
[8] L. Michels, J. O. Fossum, Z. Rozynek, H. Hemmen, K. Rustenberg, P. A. Sobas, G. N. Kalantzopoulos, K. D. Knudsen, M. Janek, T. S. Plivelic, G. J. da Silva, *Sci. Rep.* **2015**, *5*, 8775.

[9] A. B. Grommet, M. Feller, R. Klajn, *Nat. Nanotechnol.* **2020**, *15*, 256–271.
[10] J. C. Orr, V. J. Fabry, O. Aumont, L. Bopp, S. C. Doney, R. A. Feely, A. Gnanadesikan, N. Gruber, A. Ishida, F. Joos, R. M. Key, K. Lindsay, E. Maier-Reimer, R. Matear, P. Monfray, A. Mouchet, R. G. Najjar, G.-K. Plattner, K. B. Rodgers, C. L. Sabine, J. L. Sarmiento, R. Schlitzer, R. D. Slater, I. J. Totterdell, M.-F. Weirig, Y. Yamanaka, A. Yool, *Nature* **2005**, *437*, 681–686.
[11] P. M. Haugan, H. Drange, *Nature* **1992**, *357*, 318–320.
[12] W. Hage, K. R. Liedl, A. Hallbrucker, E. Mayer, *Science (80-.).* **1998**, *279*, 1332–1335.
[13] H. A. Al-Hosney, V. H. Grassian, *J. Am. Chem. Soc.* **2004**, *126*, 8068–8069.
[14] A. Ridgwell, R. E. Zeebe, *Earth Planet. Sci. Lett.* **2005**, *234*, 299–315.
[15] O. Hoegh-Guldberg, P. J. Mumby, A. J. Hooten, R. S. Steneck, P. Greenfield, E. Gomez, C. D. Harvell, P. F. Sale, A. J. Edwards, K. Caldeira, N. Knowlton, C. M. Eakin, R. Iglesias-Prieto, N. Muthiga, R. H. Bradbury, A. Dubi, M. E. Hatziolos, *Science (80-.).* **2007**, *318*, 1737–1742.
[16] N. R. Jena, P. C. Mishra, *Theor. Chem. Acc.* **2005**, *114*, 189–199.
[17] N. M. Tho, T. K. Ha, *J. Am. Chem. Soc.* **1984**, *106*, 599–602.
[18] M. T. Nguyen, M. H. Matus, V. E. Jackson, V. T. Ngan, J. R. Rustad, D. A. Dixon, *J. Phys. Chem. A* **2008**, *112*, 10386–10398.
[19] T. Loerting, C. Tautermann, R. T. Kroemer, I. Kohl, A. Hallbrucker, E. Mayer, K. R. Liedl, *Angew. Chemie Int. Ed.* **2000**, *39*, 891–894.
[20] T. Loerting, J. Bernard, *ChemPhysChem* **2010**, *11*, 2305–2309.
[21] C. S. Tautermann, A. F. Voegele, T. Loerting, I. Kohl, A. Hallbrucker, E. Mayer, K. R. Liedl, *Chem. – A Eur. J.* **2002**, *8*, 66–73.
[22] A. Stirling, I. Pápai, *J. Phys. Chem. B* **2010**, *114*, 16854–16859.
[23] D. Polino, E. Grifoni, R. Rousseau, M. Parrinello, V.-A. Glezakou, *J. Phys. Chem. A* **2020**, *124*, 3963–3975.
[24] B. Wang, Z. Cao, *J. Comput. Chem.* **2013**, *34*, 372–378.
[25] J. Meier, G. Schwarzenbach, *Helv. Chim. Acta* **1957**, *40*, 907–917.
[26] E. Magid, B. O. Turbeck, *Biochim. Biophys. Acta - Gen. Subj.* **1968**, *165*, 515–524.
[27] Y. Pocker, D. W. Bjorkquist, *J. Am. Chem. Soc.* **1977**, *99*, 6537–6543.
[28] X. Wang, W. Conway, R. Burns, N. McCann, M. Maeder, *J. Phys. Chem. A* **2010**, *114*, 1734–1740.
[29] G. Günther, J. Prass, O. Paris, M. Schoen, *Phys. Rev. Lett.* **2008**, *101*, 86104.
[30] R. Hartkamp, A. Ghosh, T. Weinhart, S. Luding, *J. Chem. Phys.* **2012**, *137*, 44711.
[31] G. Algara-Siller, O. Lehtinen, F. C. Wang, R. R. Nair, U. Kaiser, H. A. Wu, A. K. Geim, I. V Grigorieva, *Nature* **2015**, *519*, 443–445.
[32] Z. Gao, N. Giovambattista, O. Sahin, *Sci. Rep.* **2018**, *8*, 6228.
[33] A. W. Knight, P. Ilani-Kashkouli, J. A. Harvey, J. A. Greathouse, T. A. Ho, N. Kabengi, A. G. Ilgen, *Environ. Sci. Nano* **2020**, *7*, 68–80.
[34] J. A. Greathouse, T. J. Duncan, A. G. Ilgen, J. A. Harvey, L. J. Criscenti, A. W. Knight, *Environ. Sci. Nano* **2021**, *8*, 1992–2005.
[35] D. J. Bonthuis, S. Gekle, R. R. Netz, *Phys. Rev. Lett.* **2011**, *107*, 166102.
[36] D. Muñoz-Santiburcio, D. Marx, *Phys. Rev. Lett.* **2017**, *119*, 56002.
[37] F. Deißenbeck, C. Freysoldt, M. Todorova, J. Neugebauer, S. Wippermann, *Phys. Rev. Lett.*

2021, *126*, 136803.
[38] E. Chiavazzo, M. Fasano, P. Asinari, P. Decuzzi, *Nat. Commun.* **2014**, *5*, 3565.
[39] A. Phan, A. Striolo, *J. Phys. Chem. Lett.* **2020**, *11*, 1814–1821.
[40] D. Muñoz-Santiburcio, D. Marx, *Chem. Sci.* **2017**, *8*, 3444–3452.
[41] S. Biswas, H. Kwon, K. C. Barsanti, N. Myllys, J. N. Smith, B. M. Wong, *Phys. Chem. Chem. Phys.* **2020**, *22*, 26265–26277.
[42] E. Grifoni, G. Piccini, J. A. Lercher, V.-A. Glezakou, R. Rousseau, M. Parrinello, *Nat. Commun.* **2021**, *12*, 2630.
[43] L. R. Pestana, H. Hao, T. Head-Gordon, *Nano Lett.* **2020**, *20*, 606–611.
[44] C. H. Turner, J. K. Johnson, K. E. Gubbins, *J. Chem. Phys.* **2001**, *114*, 1851–1859.
[45] E. E. Santiso, A. M. George, C. H. Turner, M. K. Kostov, K. E. Gubbins, M. Buongiorno-Nardelli, M. Sliwinska-Bartkowiak, *Appl. Surf. Sci.* **2005**, *252*, 766–777.
[46] R. A. Schoonheydt, C. T. Johnston, in *Handb. Clay Sci.* (Eds.: F. Bergaya, G.B.T.-D. in C.S. Lagaly), Elsevier, **2013**, pp. 139–172.
[47] M. G. Muraleedharan, H. Asgar, S. H. Hahn, N. Dasgupta, G. Gadikota, A. C. T. van Duin, *ACS Earth Sp. Chem.* **2021**, *5*, 1006–1019.
[48] Z. Jia, Q. Wang, C. Zhu, G. Yang, in (Eds.: M.M. Rahman, A.M. Asiri), IntechOpen, Rijeka, **2016**, p. Ch. 5.
[49] N. Mendel, D. Sîretanu, I. Sîretanu, D. W. F. Brilman, F. Mugele, *J. Phys. Chem. C* **2021**, *125*, 27159–27169.
[50] K. W. Bø Hunvik, P. Loch, D. Wallacher, A. Kirch, L. P. Cavalcanti, M. Rieß, M. Daab, V. Josvanger, S. Grätz, F. Yokaichiya, K. D. Knudsen, C. Rodrigues Miranda, J. Breu, J. O. Fossum, *Langmuir* **2021**, *37*, 14491–14499.
[51] X. Dai, C. Wei, M. Wang, Y. Song, R. Chen, X. Wang, X. Shi, V. Vandeginste, *J. CO2 Util.* **2022**, *64*, 102161.
[52] A. O. Yazaydin, G. M. Bowers, R. J. Kirkpatrick, *Phys. Chem. Chem. Phys.* **2015**, *17*, 23356–23367.
[53] R. T. Cygan, V. N. Romanov, E. M. Myshakin, *J. Phys. Chem. C* **2012**, *116*, 13079–13091.
[54] C. M. Tenney, R. T. Cygan, *Environ. Sci. Technol.* **2014**, *48*, 2035–2042.
[55] Y. Li, M. Chen, H. Tang, S. Han, H. Song, P. Wang, Y. Zhao, J. Zhu, *ACS Sustain. Chem. Eng.* **2022**, *10*, 6358–6369.
[56] Z. Jin, A. Firoozabadi, *Fluid Phase Equilib.* **2014**, *382*, 10–20.
[57] J. S. Loring, E. S. Ilton, J. Chen, C. J. Thompson, P. F. Martin, P. Bénézeth, K. M. Rosso, A. R. Felmy, H. T. Schaef, *Langmuir* **2014**, *30*, 6120–6128.
[58] E. G. Krukowski, A. Goodman, G. Rother, E. S. Ilton, G. Guthrie, R. J. Bodnar, *Appl. Clay Sci.* **2015**, *114*, 61–68.
[59] T.-B. Hur, J. P. Baltrus, B. H. Howard, W. P. Harbert, V. N. Romanov, *Int. J. Greenh. Gas Control* **2013**, *13*, 149–155.
[60] S. M. Mutisya, A. G. Kalinichev, *Miner.* **2021**, *11*, DOI 10.3390/min11050509.
[61] N. Stolte, R. Hou, D. Pan, *Nat. Commun.* **2022**, *13*, 5932.
[62] M.-S. Lee, B. Peter McGrail, R. Rousseau, V.-A. Glezakou, *Sci. Rep.* **2015**, *5*, 14857.
[63] A. C. T. van Duin, S. Dasgupta, F. Lorant, W. A. Goddard, *J. Phys. Chem. A* **2001**, *105*, 9396–9409.
[64] T. P. Senftle, S. Hong, M. M. Islam, S. B. Kylasa, Y. Zheng, Y. K. Shin, C. Junkermeier, R.

Engel-Herbert, M. J. Janik, H. M. Aktulga, T. Verstraelen, A. Grama, A. C. T. van Duin, *npj Comput. Mater.* **2016**, *2*, 15011.
[65] O. Rahaman, A. C. T. van Duin, W. A. I. I. I. Goddard, D. J. Doren, *J. Phys. Chem. B* **2011**, *115*, 249–261.
[66] D. Furman, F. Dubnikova, A. C. T. van Duin, Y. Zeiri, R. Kosloff, *J. Phys. Chem. C* **2016**, *120*, 4744–4752.
[67] S. Monti, A. Corozzi, P. Fristrup, K. L. Joshi, Y. K. Shin, P. Oelschlaeger, A. C. T. van Duin, V. Barone, *Phys. Chem. Chem. Phys.* **2013**, *15*, 15062–15077.
[68] N. Dasgupta, C. Chen, A. C. T. van Duin, *Phys. Chem. Chem. Phys.* **2022**, *24*, 3322–3337.
[69] N. Dasgupta, Y. Kyung Shin, M. V Fedkin, A. C. T. van Duin, *Comput. Mater. Sci.* **2020**, *172*, 109349.
[70] M. Y. Sengul, C. A. Randall, A. C. T. van Duin, *J. Chem. Phys.* **2018**, *148*, 164506.
[71] A. Barducci, G. Bussi, M. Parrinello, *Phys. Rev. Lett.* **2008**, *100*, 20603.
[72] G. Fiorin, M. L. Klein, J. Hénin, *Mol. Phys.* **2013**, *111*, 3345–3362.
[73] S. Plimpton, *J. Comput. Phys.* **1995**, *117*, 1–19.
[74] W. E, W. Ren, E. Vanden-Eijnden, *Chem. Phys. Lett.* **2005**, *413*, 242–247.
[75] W. E, W. Ren, E. Vanden-Eijnden, *J. Phys. Chem. B* **2005**, *109*, 6688–6693.
[76] K. Adamczyk, M. Prémont-Schwarz, D. Pines, E. Pines, E. T. J. Nibbering, *Science (80-.).* **2009**, *326*, 1690–1694.
[77] D. Pines, J. Ditkovich, T. Mukra, Y. Miller, P. M. Kiefer, S. Daschakraborty, J. T. Hynes, E. Pines, *J. Phys. Chem. B* **2016**, *120*, 2440–2451.
[78] M. T. Nguyen, G. Raspoet, L. G. Vanquickenborne, P. T. Van Duijnen, *J. Phys. Chem. A* **1997**, *101*, 7379–7388.
[79] K. I. Peterson, W. Klemperer, *J. Chem. Phys.* **1984**, *80*, 2439–2445.
[80] G. A. Gallet, F. Pietrucci, W. Andreoni, *J. Chem. Theory Comput.* **2012**, *8*, 4029–4039.
[81] J. Bernard, M. Seidl, I. Kohl, K. R. Liedl, E. Mayer, Ó. Gálvez, H. Grothe, T. Loerting, *Angew. Chemie Int. Ed.* **2011**, *50*, 1939–1943.
[82] C. A. Schwerdtfeger, D. A. Mazziotti, *J. Phys. Chem. A* **2011**, *115*, 12011–12016.
[83] S. Biswas, B. M. Wong, *J. Mol. Liq.* **2021**, *330*, 115624.